This is the ACCEPTED MANUSCRIPT of the paper:
G. Petrone, W. Zamboni, G. Spagnuolo, "An interval arithmetic-based method for parametric identification of a fuel cell equivalent circuit model", Applied Energy, Volume 242, 15 May 2019, Pages 1226-1236, doi 10.1016/j.apenergy.2019.03.136

An Interval Arithmetic-Based Method for Parametric Identification of a Fuel Cell Equivalent Circuit Model

Giovanni Petrone , Walter Zamboni, Giovanni Spagnuolo

[a]*Dip. di Ingegneria dell'Informazione ed Elettrica e Matematica Applicata (D.I.E.M.), Università degli studi di Salerno - Italy*

Abstract

This paper presents an evolutionary algorithm for the online parametric identification of equivalent electric circuits representing a polymer electrolyte membrane fuel cell stack. The algorithm works on electrochemical impedance spectra. It performs a preliminary data analysis in order to account for the dependencies among the parameters and to reduce the extension of the searching space. The algorithm adopts sub-populations to improve the exploration capability of the parameter space. The normalization of the objective function improves the exploitation of the individuals. Some experimental results, obtained by running the algorithm on a low-cost embedded system, prove its convergence properties. The low computational time and the limited need of resources make the method very appealing for online diagnostic purposes.

Keywords: Fuel Cell, Interval Arithmetic, Parameter Identification.

*corresponding author

Email addresses: gpetrone@unisa.it (Giovanni Petrone), wzamboni@unisa.it (Walter Zamboni), gspagnuolo@unisa.it (Giovanni Spagnuolo)

An Interval Arithmetic-Based Method for Parametric Identification of a Fuel Cell Equivalent Circuit Model

Giovanni Petrone*, Walter Zamboni, Giovanni Spagnuolo

[a]*Dip. di Ingegneria dell'Informazione ed Elettrica e Matematica Applicata (D.I.E.M.), Università degli studi di Salerno - Italy*

Abstract

This paper presents an evolutionary algorithm for the online parametric identification of equivalent electric circuits representing a polymer electrolyte membrane fuel cell stack. The algorithm works on electrochemical impedance spectra. It performs a preliminary data analysis in order to account for the dependencies among the parameters and to reduce the extension of the searching space. The algorithm adopts sub-populations to improve the exploration capability of the parameter space. The normalization of the objective function improves the exploitation of the individuals. Some experimental results, obtained by running the algorithm on a low-cost embedded system, prove its convergence properties. The low computational time and the limited need of resources make the method very appealing for online diagnostic purposes.

Keywords: Fuel Cell, Interval Arithmetic, Parameter Identification.

*corresponding author

Email addresses: gpetrone@unisa.it (Giovanni Petrone), wzamboni@unisa.it (Walter Zamboni), gspagnuolo@unisa.it (Giovanni Spagnuolo)

1. Introduction

Polymer Electrolyte Membrane (PEM) Fuel cells (FCs) are more and more involved in energy systems as primary sources of electrical power, as well as for combined heat and power plants [1]. One of the main aspects limiting their large employment, for stationary and automotive applications, is their limited reliability. A number of possible faults is documented in literature and some research efforts are aimed at monitoring, diagnosis and prognosis of PEM-FCs [2, 3]. Also many European H2020 projects (e.g., [4]) are focused on these aspects. They face the challenging task of the development of new hardware and software tools allowing to perform diagnostic and prognostic features online, without disconnecting the FC from the load, and without using any expensive laboratory equipment.

A large number of diagnostic methods is based on the analysis of the FC impedance spectrum, obtained by the so-called Electrochemical Impedance Spectroscopy (EIS). The FC stack operating point is perturbed and the voltage and current at its terminals are measured. A small signal, usually superimposed to the stack current, is as simple as a sequence of sinusoids in an assigned frequency range. Other stimuli, having a wider frequency content, are also used. Under the hypothesis that the stack behavior is linear close to the fixed operating point, the impedance value in the assigned frequency range is computed from the voltage and current and plotted usually in the Nyquist plane (impedance plot), with the frequency as a parameter [5, 6].

The variation of the impedance spectrum often indicates a variation of the stack operating condition, or a fault, as shown, for example, in [7] for various FC operating conditions. Some data-driven methods work on the

spectrum deformations with a black- or a grey-box approach, while model-based diagnostic methods have the goal of identifying the parameters of suitable frequency-domain FC models, for instance the equivalent circuit ones, starting from the experimental impedance spectrum, as shown, for instance, in the overview paper [8] and in references therein. In these cases, the type of fault is identified by the variation of an identified parameter (or a group of them) with respect to its value in normal operating condition [7, 9]. Such approaches require an accurate circuit model of the FC stack, capable of describing the main electrochemical dynamics with simple complex-valued expressions, such as the Fouquet model [10]. Algorithms oriented to real-time diagnostics require a good compromise between speed and accuracy, and rarely are based on EIS spectra in the recent literature, as time-domain approaches are preferred. For instance, in [11], a recursive least square identification is performed starting from time-domain data under load variation, while in [12] an adaptive differential evolution algorithm is used to fit voltage-to-current curve of PEM FC models. The diagnosis is performed by using fuzzy logic and expert knowledge in [13].

The identification methods based on the experimental EIS spectrum and presented in literature often are optimization algorithms, both deterministic and stochastic ones. They are aimed at minimizing a suitable distance between the identified and experimental impedance spectra. Significant examples are given in [6] and in references therein. The quality of the identification is often dependent on the guess solution, in case a deterministic algorithm is used, or on the operators used for the solutions space exploration, if a stochastic approach is preferred. In both cases, the impedance plot derived

by the set of identified parameters might fit the experimental one with uneven accuracy in the frequency range of interest. This could be caused by an inadequateness of the equivalent circuit model, but this cannot emerge from the analysis. Moreover, the uncertainty on the experimental data cannot be taken into account during the identification process.

An alternative approach to identification problems is based on the Interval Arithmetic (IA), that is a range method proposed in literature about sixty years ago [14]. It was introduced to keep into account the rounding error arising from numerical computation, but afterwards it was also used in engineering for the determination of the tolerance's effects and uncertainties affecting some system parameters on the output of the system thereof. Recent literature acknowledges that IA-based methods are still under development, even in hybrid methods, such as the hybrid IA-particle swarm optimisation algorithm, developed for constrained optimisation problems in [15]. IA-based parameter identification is also used very recently in engineering applications, such as structural dynamic problems [16] and inverse electromagnetic design [17]. More closely to FC applications, IA is used in control-oriented modelling [18], in thermal subsystems [19] or in FC thermal behaviour analysis, typically to deal with an imperfect system knowledge and orienting the method for time-domain problems [20, 21].

The IA approach is a deterministic method. Non-IA deterministic optimization methods, aimed at finding the set of parameters that minimizes the distance between the experimental EIS data and the simulated one, are often gradient-based approaches. For these methods, the effect of the guess solution on their convergence rate and ability is well-known (e.g., [22]). The

IA-based methods, although deterministic, overcome this limitation by requiring the definition of the search space in terms of an hyper-rectangle, whose dimension is the number N_p of parameters.

This paper introduces a novel approach to face the challenging problem of the EIS-based circuit parameter identification in the frequency domain. For the first time, IA is used for this problem. The IA-based application discussed here deeply differs from the aforementioned applications [18, 19, 20, 21], that are neither based on EIS spectra, nor having a diagnostic-oriented outcome. The method is based on a Branch and Bound (B&B) algorithm, working with the so-called interval value parameters. A suitable smart contraction operator is developed, so that the subsets of the initial search space that do not contain the experimental data are discarded progressively. This is done in a reliable way, because IA properties guarantee that in those subsets no solution falls, and efficiently, with a reduced computational burden and memory requirements. For each parameter, an interval of feasible values, instead of a real number, is the result of the identification. The method is further enhanced with a relaxed feasibility condition allowing to treat noisy EIS data properly, especially at low frequency. The results of the proposed IA-based identification method is validated in some reference cases and applied to case studies of practical interest for the PEM FC EIS framework.

The proposed deterministic algorithm achieves a valuable reduction of computational burden and memory requirements with respect to the basic B&B algorithm. In fact, it is oriented towards online FC diagnostics, that can also be performed with low-cost embedded systems. Indeed, for such kind of analysis, the interval representation of parameters allows to analyse their

variation in a compact way. This allows an easier identification of correlations existing between monitored parameters and degradation phenomena, thus providing a timely counteraction for preserving the system reliability and durability.

It is worth to highlight the meaning of the interval representation of parameters. Thanks to the IA properties, the interval is intended in a worst case sense [14]. Conversely, literature papers dealing with FC parameter identification and diagnostics, e.g., [23, 24], use confidence intervals in a statistical sense, because these intervals come out from signal processing, highlighting inaccuracy of EIS measurement especially in low frequency range [25]. The latter effects are automatically taken into account by IA. Moreover, using IA, the sensitivity of the FC frequency response with respect to the whole set of parameters comes out clearly. Such a feature makes the algorithm of great interest for detecting stack malfunctioning and parametric drifts, which can be the symptoms of future faults. Thus, the method allows to act on the feedback control of the FC stack parameters to improve its lifetime, quality of the energy conversion, and efficiency.

To the authors' knowledge, the basic IA-based B&B algorithm (that will be recalled in Section 4.1) was applied to some systems [26], but its straightforward use to the FC spectrum identification for pursuing diagnostic objectives does not give useful results. This paper is aimed at showing such a limitation, and at demonstrating that the proposed Enhanced Smart B&B approach (hereafter called ESB&B) ensures more reliable and useful results.

The paper is organized as follows. In Section 2, a brief overview of the main features offered by IA in parametric identification is given, Section 3

presents the adopted FC model (Fouquet model), Section 4 describes the IA-analisys B&B algorithm, discussed and validated in Section 5. Then, the ESB&B is proposed in Section 6 and applied in Section 7. In Section 8, the results are discussed in the perspective of FC diagnosis as well as for other applications, showing the benefits of such an approach, and, finally, some conclusions are drawn in Section 9.

2. Interval arithmetic and parametric identification

IA is funded on the following principle: each variable or parameter in a system, X, is defined by the range of the real values it can assume, that is an *interval*, in the following always denoted by the square brackets: $[X]$. Thus the interval $[X]$ is defined as an ordered pair of real numbers a, b such that $[X] = [a, b] = \{x | a \leq x \leq b; \quad x, a, b \in \mathbb{R}\}$, all the values in $[X]$ being equally probable. Given a function y of N_p interval-valued parameters, the codomain of the function is an interval $[Y] = f([X_1], \cdots, [X_{N_p}])$, with $[X_h] = [a_h, b_h]$. If y is expressed in a closed-form, $[Y]$ can be calculated straightforwardly by applying the *interval extension* of the elementary functions appearing in f. The main feature of IA is that the result of the *interval extension* of any elementary function is an interval that is guaranteed to include all possible values of that function in its domain.

As an example, the subtraction between the two intervals $[X_1]$ and $[X_2]$ is calculated as follows:

$$[Y] = [X_1] - [X_2] = [a_1 - b_2, b_1 - a_2] \tag{1}$$

Such an example highlights that the result of the IA calculation is eas-

ily determined, but the drawback is that $[Y]$ might be larger than the real codomain. This is evident if the subtraction $[X_1] - [X_1]$ is performed, whose result should be the degenerate interval $[0, 0]$, but IA is not able to distinguish the difference $[X_1] - [X_1]$ from the difference between two intervals $[X_1]$ and $[X_2]$ having the same extremes, thus $a_1 = a_2$ and $b_1 = b_2$, but representing uncorrelated interval variables. These IA drawbacks are called *wrapping effect* and *dependency error*. They cause an overestimation of the function codomain [26]. Wrapping the range of variation of the function always into an hyper-rectangle is a IA feature, so that wrappings with a more involved shape cannot be described with a so simple entity as the real interval is. Furthermore, the missed correlation among different instances of the same uncertain variable gives an overestimation error of the function codomain that is much more evident as higher is the number of occurrences of the variable thereof.

For instance, the codomain of the second order polynomial $y = x^2 - 5x + 2$ over the interval $[X] = [1, 2]$ gives $[Y] = [-7, 1]$ if the interval $[X]$ is merely substituted into the polynomial expression and the calculations are done according to the IA rules. Instead, if the polynomial is put in the form $y = x(x - 5) + 2$ and the same IA operations are done, the result becomes $[Y] = [-6, -1]$, which is more accurate than the previous one. The reason of this discrepancy is in the number of occurrences of the interval variable x in the former expression. This example reveals that a suitable symbolic processing of the function expression on which the IA may achieve more accurate results. In conclusion, the advantage in adopting the IA for evaluating the codomain of a function of a number of variables is that it is calculated by substituting to

each variable its interval and to use the interval extension of all the operations involved in the function. The resulting interval is guaranteed to contain the codomain of the function. The codomain overestimation provided by IA is small if the incidence of the *wrapping effect* and of the *dependency error* are limited through a proper implementation of the IA extension of the function, further details about these issues can be found in [26].

3. Fuel cell model

Many algorithms are used for the identification of equivalent circuit parameters that accurately model the PEM FC behavior. The most used one is the Fouquet equivalent circuit [10]. It models the charge transfer and the mass transport phenomena by means of the Warburg element, which accounts for diffusion phenomena, and by the Constant Phase Element (CPE), which accounts for the distribution of electrolyte microscopic capacitive properties [10]. In Figure 1 the Fouquet model is shown and the corresponding equation of the impedance in the frequency domain is given by (2).

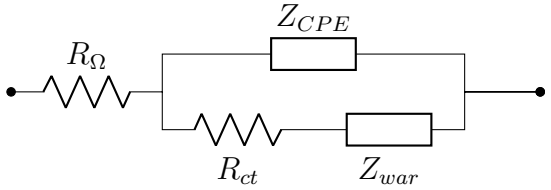

Figure 1: Fouquet model

$$\dot{Z}_{\mathrm{F}} = R_\Omega + \frac{\dot{Z}_{CPE}(R_{ct} + \dot{Z}_W)}{\dot{Z}_{CPE} + R_{ct} + \dot{Z}_W} \tag{2}$$

where

$$\dot{Z}_{war}(\omega) = R_D \frac{\tanh(\sqrt{j\omega\tau_D})}{\sqrt{j\omega\tau_D}}$$
$$\dot{Z}_{CPE}(\omega) = \frac{1}{Q(j\omega)^{\phi}}$$

The model includes the following $N_p = 6$ parameters:

- R_Ω, representative of losses due to the resistance of the electrolyte to the transit of protons H^+.
- R_{ct}, charge transfer resistance, is the resistance imposed by the interface electrode/electrolyte to the transit of charges.
- R_D, representative of losses due to the diffusion of reactants. With τ_D, it is part of the Warburg element.
- Q, with ϕ, is representative of the CPE, which models the behavior of electrodes in case of rough and porous surfaces.
- ϕ, coefficient between -1 and 1.
- τ_D diffusion time constant of Warburg element.

Finally, introducing the vector of $N_p = 6$ parameters:

$$\mathbf{P} = (R_\Omega, R_{ct}, R_D, Q, \phi, \tau_D)\,, \tag{3}$$

the Fouquet impedance can be written as a function of the angular frequency ω and of the parameters:

$$\dot{Z}_{\mathrm{F}}(\mathbf{P},\omega) = R_{\Omega} + \left[\left(R_{ct} + R_D \frac{\tanh(\sqrt{j\omega\tau_D})}{\sqrt{j\omega\tau_D}}\right)^{-1} + Q(j\omega)^{\phi}\right]^{-1}. \qquad (4)$$

It is worth to notice that (4) is written by minimizing the number of occurrences of each interval variable, so that the *wrapping effect* and *dependency error* are minimized.

4. The branch and bound algorithm

For the development of the IA-based identification method, it is assumed that the FC impedance $\dot{Z}_{\mathrm{exp}}$ is given, e.g., through experimental measurements, in a number N of angular frequency values $\{\omega_1, \ldots, \omega_N\}$. Let $R_{\mathrm{exp},k}$ and $X_{\mathrm{exp},k}$ be the real and imaginary part of the kth impedance value, $k = 1, ..., N$:

$$R_{\mathrm{exp},k} = \Re\left\{\dot{Z}_{\mathrm{exp}}(\omega_k)\right\}, \qquad (5a)$$

$$X_{\mathrm{exp},k} = \Im\left\{\dot{Z}_{\mathrm{exp}}(\omega_k)\right\}. \qquad (5b)$$

The objective of the IA-based algorithm is to find the smallest interval for each component of the vector of parameters $\mathbf{P}$ such that the interval values of the real and of the imaginary part of the Fouquet impedance function $\dot{Z}_{\mathrm{F}}$ include all the experimental measurements (5). In symbols, the smallest interval vector $[\mathbf{P}]$ has to be found, ensuring that the following constraints are fulfilled:

Feasibility condition

$$R_{\mathrm{exp},k} \in [R_{\mathrm{F}}(\mathbf{P}, \omega_k)] \quad \text{for all } k = 1, \ldots, N \tag{6a}$$

$$X_{\mathrm{exp},k} \in [X_{\mathrm{F}}(\mathbf{P}, \omega_k)] \tag{6b}$$

so that each measured experimental value belongs to the identified interval of the Fouquet impedance. If wide intervals are used for $[\mathbf{P}]$, the Fouquet impedance intervals appearing on the right-hand sides of (6) might be so large that all those constraints are fulfilled. Starting from such a feasible set, called $[\mathbf{P}]_0$, the Branch and Bound (B&B) loop is designed.

The idea underlying the B&B approach can be explained by means of the intuitive two-dimensional (2D) example shown in Figure 2. In this case, the intervals initially chosen for (p_1, p_2) give the initial search space $[\mathbf{P}]_0$ (outer grey rectangle). Given the experimental data (white markers of the system performance function) and the related measurement noise (bars for each white marker), the goal of the IA approach is to find the smallest envelope of the red band that is the codomain of $f(\mathbf{P}, \omega)$, obtained with the corresponding $[\mathbf{P}]_f$ in the parameters domain. By branching the search space $[\mathbf{P}]_0$ in sub-intervals and by calculating the corresponding interval codomains, it is possible to discard the unfeasible sub-intervals, in such a way that the initial search space is progressively contracted towards $[\mathbf{P}]_f$ (inner grey rectangle). It is worth to note that, for the N_p-dimensional identification problem, $[\mathbf{P}]_f$ is an N_p-dimensional hyper-rectangle.

4.1. Basic B&B algorithm

In [26], the basic B&B algorithm is extensively presented and its appli-

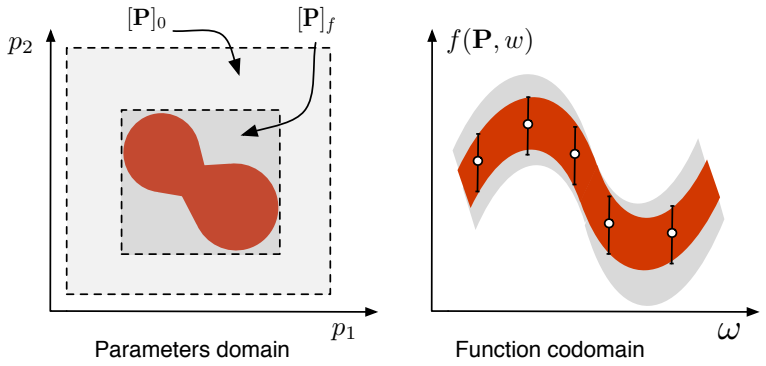

Figure 2: Basic example of B&B IA-based method for parameters estimation

cation to some basic problems is commented. Here, the B&B algorithm is briefly resumed.

At each ith loop step ($i > 0$), called *branching level*:

Step 1. Branching. All the interval components $[p_h]_{i-1}$ of $[\mathbf{P}]_{i-1}$ are halved at the ith level, so that each interval valued parameter is the union of two smaller intervals, that are the left-hand side $[p_h^L]_i$ and the right-hand side $[p_h^R]_i$ semi intervals of the original one. In symbols:

$$[p_h]_{i-1} = [p_h^L]_i \cup [p_h^R]_i \qquad h \in \{1, \ldots, 6\}. \tag{7}$$

It is evident that the combination of the left and right side intervals in (7) gives rise to 2^6 parameters subsets, whose union gives the original six-dimensional (6D) hyper-rectangle $[\mathbf{P}]_{i-1}$.

Step 2. Checking feasibility. The evaluation of the Fouquet impedance (4) for each one of these 2^6 subsets allows to classify them in terms of feasibility. The IA extension of (4), evaluated at each angular frequency, gives the interval codomains $[R_{\mathrm{F}}(\mathbf{P}, \omega_k)]$ and $[X_{\mathrm{F}}(\mathbf{P}, \omega_k)]$. Each parameters subset fulfilling

all the feasibility conditions (6) will be called *feasible subset*, while a subset not fulfilling *at least one* of the feasibility conditions will be called *unfeasible subset*.

Step 3. Discarding unfeasible subsets. Unfeasible subsets can be definitely discarded. This result is guaranteed by the inherent IA property of inclusion of the codomain of an interval-valued function. Such a key property allows to neglect entire subsets of the search space without any further investigation. Indeed, the interval extensions R_F and X_F are guaranteed to contain all the possible combinations of the results which might be obtained by a value-by-value evaluation through the real calculation. Thus, if the interval extensions do not fulfill (6), then it is guaranteed that the experimental values of the spectrum cannot be obtained by any of the combinations of the values of the parameters of that subset. Conversely, feasible subsets have to be halved furthermore and the feasibility condition to be verified in the resulting subsets. All the three steps above are repeated until a suitable convergence condition is fulfilled. From a graphical point of view, the algorithm assumes the shape of a tree, with some branches interrupted earlier than others because the corresponding subsets are unfeasible.

The termination condition is stated either in terms of a small fraction (σ_V) of the initial volume of the search space that need to be halved furthermore, or in terms of maximum branching level $L_{\max}$. In the following, $\sigma_V = 10^{-18}$ and $L_{\max} = 50$ are used. It is worth to notice that, for the 6D parametric identification discussed in this paper, by assuming a uniform segmentation, the selected σ_V is equivalent to a minimum width $w_{\min,h} = 10^{-3}$ for each parameter.

When the algorithm is terminated, the subsets that should need a further halving can be classified as *undetermined* ones. The result of the B&B algorithm is the union of all the feasible subsets.

4.2. Wrapping the solution

At a given branching level, i.e., at a given iteration, a number of subsets is feasible, so that they need a further branching and testing. Nevertheless, at that level, two current solutions to the identification problem may represent the output of the algorithm.

As it will be clarified through the examples, depending on the specific identification and diagnostic objective, the B&B algorithm can be used to find either the *wrapping region*, or the *safe region*.

For their definition, and for a clearer comprehension of the idea, it is useful to refer to a 2D case, where the feasible subsets are represented by rectangles. Considering the 2D example shown in Figure 3, where the parameters x_1 and x_2 have to be identified, it is supposed that the rectangles $P1, \ldots, P12$ all represent the feasible subsets at a given branching level. They can be *wrapped* by the rectangle representing the largest intervals of x_1, x_2, producing a codomain that, thanks to the IA properties, includes the experimental measurements. This region is called *wrapped subset*.

It is evident that, for non-connected and/or non-convex feasible regions, the *wrapped subset* includes also some unfeasible parameters subsets, that contribute to enlarge the codomain width of (4) when it is evaluated on the *wrapped subset*.

On the other side, the largest convex region $P3 - P8$ can be defined as the *safe subset*, represented by the inner rectangle. It is named safe subset

because it represents the largest rectangle of x_1, x_2 producing the smaller codomain that includes the experimental measurements. Each rectangle in the safe region is feasible, but it does not include all feasible rectangles. It

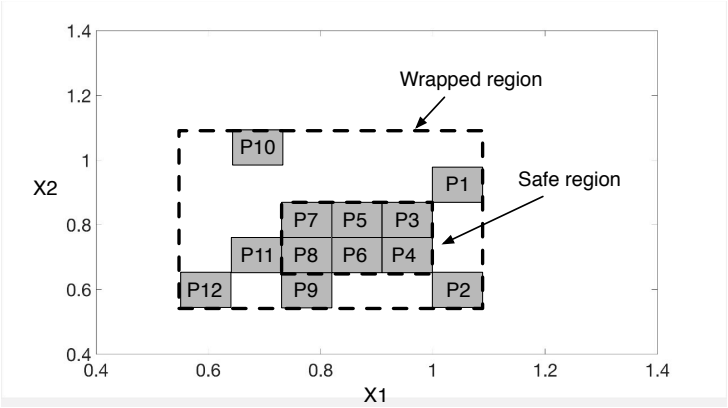

Figure 3: Wrapped and safe regions on P1-P12 subsets.

is worth to remark again that, when more than two parameters have to be identified, the subsets are no longer rectangles, but hyper-rectangles.

4.3. Smartening the B&B algorithm

The segmentation of the search space of the B&B algorithm is expected to grow exponentially with the number N_p of parameters at each branching level, although the presence of a number of unfeasible subsets allows to reduce it in an undetermined way. The high number of subsets, growing at each branching level, has to be stored in memory, tested for feasibility and halved, generating a high computational burden. In order to reduce it, the algorithm is here enhanced in the following novel way.

At each branching level, and for each subset, instead of halving the intervals of all the N_p parameters, a reduced number of subsets is generated by halving only those intervals of parameters deeply affecting the width of

the impedance spectrum. The decision is based on looking at the wrapping region and on the branching steps. More specifically, two "indices" are considered.

- The *directions of contraction* of the wrapping region W_i at the ith branching level with respect to the wrapping region W_{i-1} at the preceding level (notice that the wrapping regions are hyper-rectangles). In other words, this is an indicator of discrete local sensitivity of W_i with respect to the parameters. A binary contraction vector $\mathbf{C}_i$ is introduced, whose components $c_{i,h}$ assume binary values $\{0, 1\}$ and, if true, represents the direction of contraction from $(i-1)$th to ith level.

- The *direction of branching* at the preceding level, i.e., the set of parameters interval halved at the $(i-1)$th step. A branching direction logical vector $\mathbf{B}_i$ is introduced at each branching level, as done previously for $\mathbf{C}_i$.

At the ith level, if the wrapping region W_i comes from a contraction along some directions with respect to preceding W_{i-1}, these contraction directions are taken as branching directions for the actual step. More formally, in the case of a contraction from the $(i-1)$th and the ith levels along the hth direction, $b_{i,h} = c_{i,h} = 1$. It is worth to notice that, if h is a direction of contraction for W_i, the parameter interval $[p_h]$ could have not *necessarily* been halved in that direction. This is compatible with the well-known IA property of reducing the overestimation of the interval codomain by segmenting the interval domain, which is the interval parameters. On the other side, the smaller the intervals of codomain, the higher the number of interval param-

eter subsets that can be discarded by checking constraints (6). Hence, all subsets having the same not branched parameter $[p_h]$ might be unfeasible. This allows its contraction even if it has not been halved. In practice, the mitigation of IA wrapping effect, and the dependency error due to the halving of some parameters induces, indirectly, the contraction of the intervals of other parameters. Writing a pseudo-code, it holds:

Selective branching condition

$$\begin{aligned} &\texttt{if } W_i \subset W_{i-1} \\ &\quad \mathbf{B}_i = \mathbf{C}_i \\ &\texttt{end} \end{aligned} \tag{8}$$

When the parameters to be branched are less than N_p, the process could end up with a wrapping region that is not contracted any more, that is: $W_i = W_{i-1}$. In this case, the sensitivity vector is zero: $\mathbf{C}_i = [0, \ldots, 0]$. In this case, the branching goes on in the complementary branching directions, i.e., in the directions of parameters not branched at the previous step. For instance, if $\mathbf{C}_i = [0, \ldots, 0]$ and the previous branching directions are 1 and 3, ($\mathbf{B}_{i-1} = [1, 0, 1, 0, 0, 0]$), then the successive branching is preformed along 2, 4, 5, 6 ($\mathbf{B}_i = [0, 1, 0, 1, 1, 1]$). In a compact form:

Change direction condition

$$\begin{aligned} &\texttt{if } W_i = W_{i-1} \\ &\quad \mathbf{B}_i = \overline{\mathbf{B}}_{i-1} \\ &\texttt{end} \end{aligned} \tag{9}$$

Finally, if the *Change direction condition* does not produce any useful bounding of the wrapping region, the algorithm undergoes a reset, i.e., all parameters will be branched again from that branching level ahead.

Reset condition

$$\begin{aligned} &\texttt{if } W_i = W_{i-1} = W_{i-2} \\ &\quad \mathbf{B}_i = [1,1,1,1,1,1] \\ &\texttt{end} \end{aligned} \tag{10}$$

Summarizing, the smart B&B algoritm works as follows.

$$\begin{aligned} &\texttt{if } W_i \subset W_{i-1} \\ &\quad \mathbf{B}_i = \mathbf{C}_i \quad \textit{(smart branching)} \\ &\texttt{else} \qquad (W_i = W_{i-1}) \\ &\quad \texttt{if } W_{i-i} = W_{i-2} \\ &\quad\quad \mathbf{B}_i = [1,1,1,1,1,1] \quad \textit{(reset)} \\ &\quad \texttt{else} \\ &\quad\quad \mathbf{B}_i = \overline{\mathbf{B}}_{i-1} \quad \textit{(change direction)} \\ &\quad \texttt{end} \\ &\texttt{end} \end{aligned}$$

4.4. A 2D pilot example

In order to show how the IA-based B&B identification algorithm works, a 2D identification problem is afforded in the framework of PEM FC appli-

cation. In order to put in evidence the benefits of the proposed method, the 2D identification problem is firstly analysed without the Smart branching algorithm.

A fictitious experimental spectrum $\dot{Z}_{\text{exp}}(\omega_k)$ is generated for a number $N_f = 38$ of frequency points ω_k, as shown in Figure 4 (the parameters used to generated the plot are reported therein).

The objective of this pilot example is the identification of two parameters: $p_1 = R_\Omega$ and $p_2 = R_{ct}$, the remaining ones being fixed at their true value. This is done by launching the proposed B&B algorithm on a search space generated by the initial set $[\mathbf{P}]_0 = ([0.0001, 2.0000]\Omega, [0.0001, 2.0000]\Omega)$. Such an initial set is feasible, i.e., it contains the values $R_\Omega = 4.5\, m\Omega$ and $R_{ct} = 8.1\, m\Omega$ used to generate the plots shown in Figure 4. In this case, the search space is a square in the plane, so that the branching action of the B&B algorithm can be shown easily.

The Fouquet impedance $\dot{Z}_{\text{F}}$ is evaluated through IA over $[\mathbf{P}]_0$ for each ω_k. The corresponding intervals $[R_{\text{exp},k}]$ and $[X_{\text{exp},k}]$ are compared with the experimental data in Figure 5, showing the feasibility of $[\mathbf{P}]_0$. The first branching step is depicted in Figure 6. The Fouquet impedance is evaluated again, for all frequency points, over the four subsets depicted in Figure 6, being P1 feasible (it will be branched furthermore), and P2, P3, P4 unfeasible and discarded as a whole. Figure 7 shows the codomain associated to P3 as red lines. Notice that, for many ω_k, the depicted bars do not include the corresponding markers, both on real and imaginary plots. The reliability of this result comes from the IA inclusion property, because it guarantees that all the possible parameters combinations in P3 cannot give impedance intervals

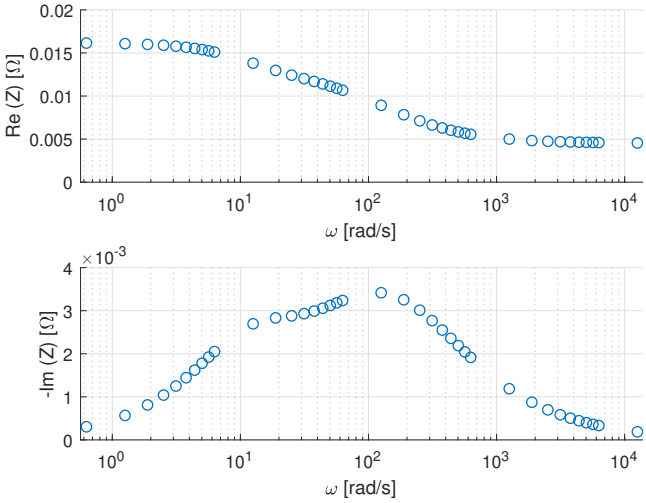

Figure 4: Pilot 2D example: real and imaginary parts of the FC impedance spectrum $\dot{Z}_{\text{exp}}$ calculated with the Fouquet model. Parameters used: $\mathbf{P}_{\text{exp}} = (0.0045\,\Omega,\ 0.0081\,\Omega,\ 0.0036\,\Omega,\ 1.8059, 0.8419, 0.1919\,\text{s})$

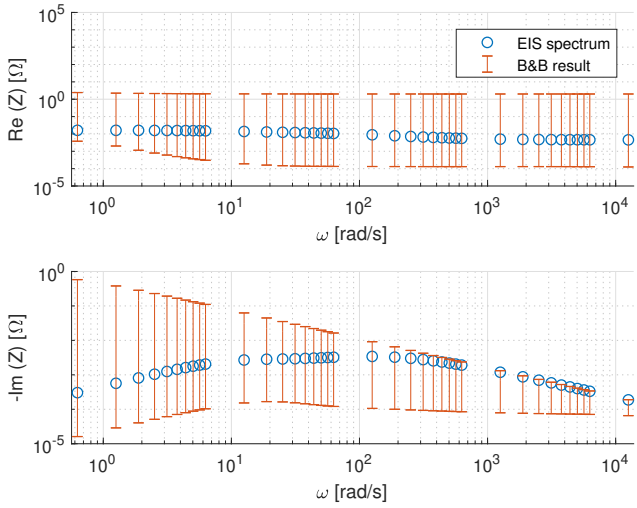

Figure 5: Pilot 2D example: log-scale codomain of the initial set $[\mathbf{P}]$ (red bars) compared with the FC impedance values (blue circles).

wider than those ones shown in Figure 7.

Successive branching of P1 lead to convergence at the 29^{th} branching

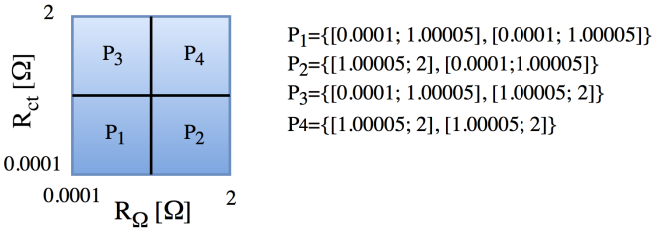

Figure 6: Pilot 2D example: P1, P2, P3 and P4 subsets after the branching action.

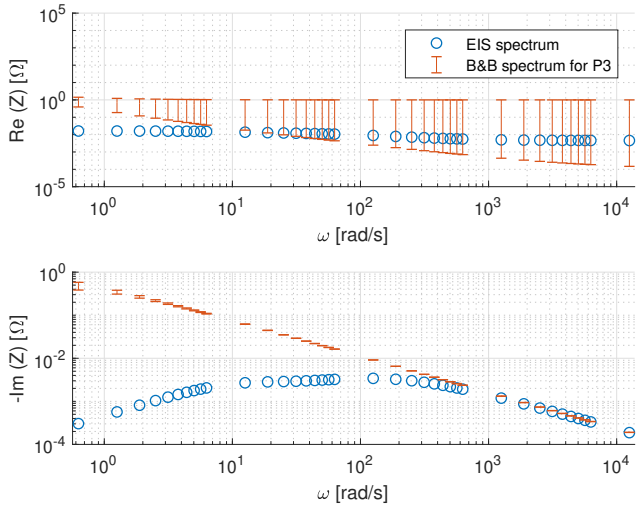

Figure 7: Pilot 2D example: codomain of the unfeasible subset P3 (red bars) compared with the emulated impedance $\dot{Z}_{\text{exp}}$ (blue circles).

level. For the sake of example, the results achieved at the fourteenth branching level, corresponding to the subset $([4.494, 4.738]m\Omega, [7.912, 8.156]m\Omega)$, is shown in Figure 8. This is the unique feasible subset to be branched furthermore. At this stage, the wrapped and the safe regions coincide with the aforementioned subset.

The spider plot shown in Figure 9 gives track of the branching process. The left-hand bounds R_{Ω}^{-} and R_{ct}^{-} are subject to a two-steps contraction in

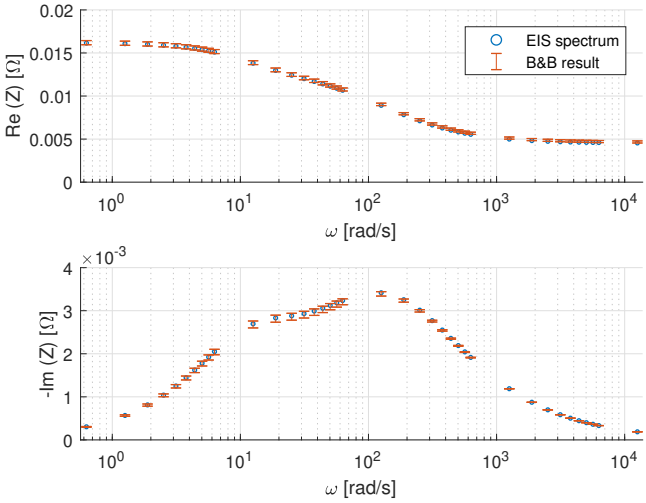

Figure 8: Pilot 2D example: codomain of the subset at the 14^{th} branching level (red bars) and impedance values used for parameters identification (blue circles).

the first branching levels, from 0.0001Ω to 0.00449Ω and from 0.0001Ω to 0.00791Ω respectively. Instead, both the upper side interval bounds are contracted more progressively, from 2Ω downwards, this showing a predominant sensitivity of the problem with respect to the upper bounds of the resistances included in the chosen initial search space.

5. B&B identification working on emulated impedance spectrum

5.1. Case study 1

In this case study, the fictitious experimental spectrum $\dot{Z}_{\text{exp}}(\omega_k)$ described in the previous section is used. The goal of the case study is to perform a full 6D identification of the Fouquet model (4), based on $\dot{Z}_{\text{exp}}(\omega_k)$ in Figure 4, by using the smart approach described in Section 4.3, starting from the following initial feasible set:

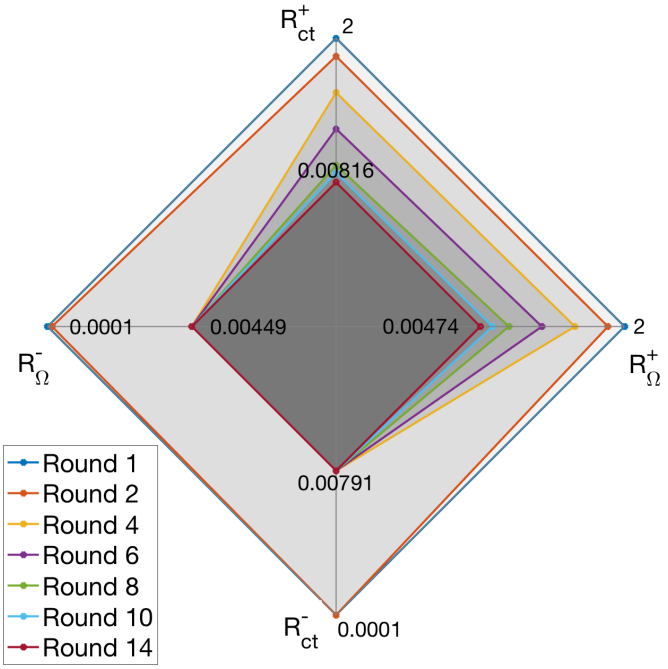

Figure 9: Pilot 2D example: IA-based contraction of the two dimensional search space (spider plot).

$$[\mathbf{P}]_0 = ([0.0001, 2.0]\,\Omega, [0.0001, 2.0]\,\Omega,\ [0.0001, 2.0]\,\Omega,$$
$$[0.1, 1.0],\ [0.1, 5.0],\ [0.1, 1.0]\,s) \tag{11}$$

$[\mathbf{P}]_0$ generates a 6D search space. The classification of the subsets obtained without applying the smart approach of Section 4.3 is shown in Table 1 for the first seven branching levels, highlighting the percentage of feasible subsets at each branching level. It is worth to notice the huge number of subsets to be processed, and whose bounds have to be stored in memory. Moreover, at the seventh level, only the interval associated to the three resistances were

effectively reduced:

$$[R_\Omega]_7 = [R_{ct}]_7 = [R_d]_7 = [0.0001, 0.0313484]\,\Omega \tag{12}$$

Branching level	**Total subsets**	**Feasible subsets**
1	1	1
2	64	9 (14.1%)
3	576	60 (10.4%)
4	3840	448 (11.7%)
5	28672	3472 (12.1%)
6	222208	26944 (12.1%)
7	1724416	212043 (12.3%)

Table 1: Case study 1: subsets classification at each branching level up to the seventh one.

If the smart approach is applied, the high numbers shown in the Table 1 fall down as shown in Table 2.

Branching level	**Total subsets**	**Feasible subsets**	**Branched parameters**
1	1	1	All
2	64	9 (14.1%)	R_Ω, R_{ct}
3	36	9 (25.0%)	R_Ω, R_{ct}
4	36	9 (25.0%)	R_Ω, R_{ct}
5	36	11 (30.6%)	R_Ω
6	22	11 (50.0%)	R_Ω
7	22	11 (50.0%)	R_Ω

Table 2: Case study 1: smart branching results up to the seventh level.

The smart B&B algorithm is able to recognize that the major contraction effects derives from the branching of $[R_\Omega]$ and $[R_{ct}]$, while the intervals of the remaining parameters are not halved. At the seventh round, the intervals of

the resistances are:

$$[R_\Omega]_7 = [0.0001, 0.0313484]\,\Omega \tag{13a}$$

$$[R_{ct}]_7 = [0.0001, 0.250088]\,\Omega \tag{13b}$$

Although the second one is larger than the one in (12), the memory usage now is significantly reduced and the result is achieved in much less computations. At the seventh branching level, it is required to store only 11 feasible subsets instead of 212043. From the seventh level, the B&B smart algorithm can continue to run and bound the parameters without any memory explosion, achieving the following solution:

$$\begin{aligned}[\mathbf{P}]_{\text{sol}} = ([4.49, 4.50]\,m\Omega,\ [8.01, 8.19]\,m\Omega,\ [3.49, 3.73]\,m\Omega,\\ [0.838, 0.845],\ [1.76, 1.85],\ [0.183, 0.20]\,s)\end{aligned} \tag{14}$$

The widths of the solution intervals (14) are narrow with respect to the center values. The smallest is $\pm 0.11\%$ for R_Ω and the largest is $\pm 4.93\%$ for τ_D.

Table 3 shows some details about the remaining branching levels up to convergence. The codomain corresponding to the solution (14) is shown in Figure 10 and compared to $\dot{Z}_{\text{exp}}$.

Figure 10 shows how tolerant such identified parameters' intervals are with respect to the possible noise affecting $\dot{Z}_{\text{exp}}$. The result (14) should be obtained also in the presence of a significant noise level affecting the imaginary part of the measured impedance in the low frequency range, where the red markers show a large range around the blue circles. Conversely, some noise affecting X_{exp} at high frequency or R_{exp} in the whole frequency

Branching level	Total subsets	Feasible subsets	Branched parameters
8	22	11	R_Ω
9	22	11	R_Ω
10	22	22	R_{ct}, Q, ϕ, R_d, τ_d
11	704	120	R_{ct}, R_d
12	480	135	R_{ct}, R_d
13	540	176	R_{ct}, R_d
14	704	249	R_{ct}
15	498	424	R_Ω, Q, ϕ, R_d, τ_d
16	13568	1905	R_Ω, R_{ct}, R_d
17	15240	2477	R_Ω, R_{ct}, R_d
18	19816	3667	R_{ct}
19	7334	5609	R_Ω, Q, ϕ, R_d, τ_d
20	179488	3727	R_Ω, R_{ct}, R_d
21	29816	3929	R_Ω, R_{ct}, Q, ϕ, R_d
22	125728	3883	All
23	248512	4461	All
24	285504	4576	All
25	292864	4488	All
26	287232	3795	All
27	242880	4709	All

Table 3: Case study 1: smart branching results from the 8^{th} to the 27^{th} level.

range would lead to a significant increase of the identified parameters interval widths. Such a result also gives a clear indication about the care required during the experimental measurements acquisition. The greater tolerance of the method at low frequencies is helpful, especially if $\dot{Z}_{\text{exp}}$ are obtained experimentally by using a sinusoid-based EIS. Indeed, it is well-known that the EIS is more critical at low frequency, where keeping the FC in a stationary operating point is an hard task. Thus, a EIS approach requiring high stability of the operating point for a very long time interval, would allow to improve also the parametric identification at low frequencies. It is worth noting that any identification method would suffer from the high noise level

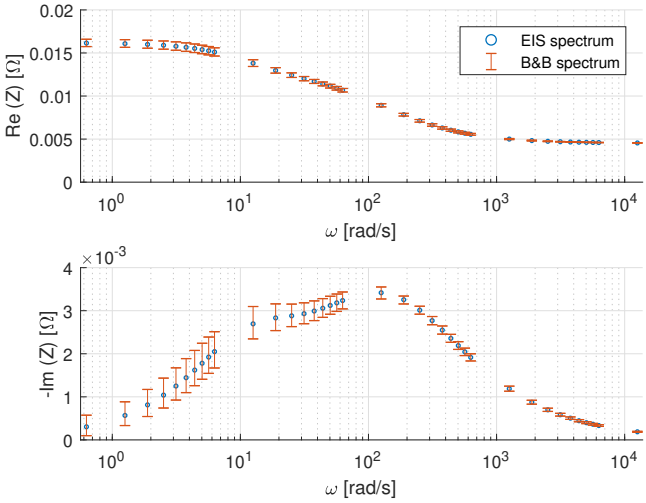

Figure 10: Case study 1: identified impedance spectrum (red ranges) obtained from the solution (14). The parameter set is feasible, i.e., the red ranges include the experimental blue markers.

at low frequencies, not only the method proposed in this paper.

An alternative analysis could be performed by studying the FC magnitude and phase response, in lieu of the real and imaginary part. This would require alternative mathematical relationship for the computation of *wrapping effect* and *dependency error* with respect to $[\mathbf{P}]$.

6. Extension of the B&B smart algorithm

The presence of noise affecting the experimental data $\dot{Z}_{\text{exp}}(\omega)$ has a deep impact on the B&B algorithm contraction ability. Indeed, the feasibility condition could not be matched in *all* the frequency point ω_k. The larger the noise affecting $\dot{Z}_{\text{exp}}$, and even only at one frequency point, the more difficult the contraction of the initial search space. The width of the intervals $[p_h]$ would keep so large that the resulting information becomes useless, even if

formally correct and feasible. To face this problem, the algorithm is here modified by introducing two innovations. First, the feasibility condition in used in an extended sense, and then, the condition is further relaxed. The novelties are detailed as follows.

6.1. Enhanced B&B smart algorithm in the presence of interval-valued experimental data

The algorithm described in 4.1 can be easily extended to the case in which, at each ω_k, a number of measurements is available. In this case, also the kth measurement set (at each frequency) can be represented by two interval-valued variables: $[R_{\mathrm{exp},k}]$, $[X_{\mathrm{exp},k}]$.

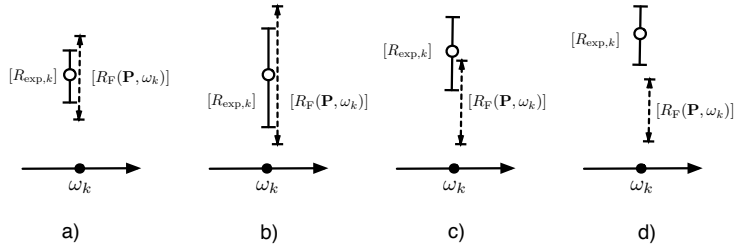

Figure 11: Qualitative analysis of the effect of noise on experimental data. a) and b) feasible cases. c) *extended sense* feasible case. d) unfeasible case.

Figure 11 shows what may happen to $[R_{\mathrm{exp},k}]$ and $[R_{\mathrm{F}}(\mathbf{P},\omega_k)]$. This is done in a qualitative way and with particular reference to the real part of the impedance at a given frequency value. In Figure 11.a) and b), the experimental interval $[R_{\mathrm{exp},k}]$ is strictly included in the one identified through the proposed IA method, $[R_{\mathrm{F}}(\mathbf{P},\omega_k)]$. In this cases, any noiseless experimental point would have been feasible. For instance, the central one is marked with a circle. Obviously, it follows that the identified set of parameters, as a whole, remains feasible. The comparison between the two cases shows that

the greater the noise, the less effective the contraction the IA method is able to perform. Figure 11.c) depicts a new case. The noiseless experimental point, again marked with a circle in the figure, would have been unfeasible. Nevertheless, it is apparent that the experimental and the identified intervals overlap. It follows that there might be a portion of Rf that cannot be classified as unfeasible. This calls for an *extended sense* definition of the feasibility condition allowing this interval to be feasible. Finally, Figure 11.d) shows the evident case in which the experimental interval is definitely unfeasible.

This figures allows one to understand the effects of noise affecting the experimental measurements. As in cases a) and b) the IA based method cannot push a further contraction of the identified intervals, the noise interval acts as an inner bound limitation to contraction. Instead, in case c), where a further branching step of the search space is required, the experimental noise allows to broaden the search space in a selective way, including regions that would have been discarded with the approach presented in the previous sections.

Such an *extended sense* feasibility conditions requires the following definition.

Extended feasibility condition.

$$[R_{\text{exp},k}] \cap [R_{\text{F}}(\mathbf{P}, \omega_k)] \neq \emptyset \quad \text{for all } k = 1, \ldots, N \tag{15a}$$

$$[X_{\text{exp},k}] \cap [X_{\text{F}}(\mathbf{P}, \omega_k)] \neq \emptyset \tag{15b}$$

As already proposed above, at each iteration, after the branching step, unfeasible subsets are definitely discarded while feasible ones are worth to be

branched furthermore. For a feasible sets (e.g., the nth), the following condition might occur at the ith branching level:

Acceptability condition.

$$[R_{\mathrm{exp},k}] \supseteq [R_{\mathrm{F}}(\mathbf{P}, \omega_k)]_{i,n} \quad \text{for all } k = 1, \ldots, N \tag{16a}$$

$$[X_{\mathrm{exp},k}] \supseteq [X_{\mathrm{F}}(\mathbf{P}, \omega_k)]_{i,n} \tag{16b}$$

In this case, the acceptable subset $[\mathbf{P}]_{i,n}$ is considered as definitely feasible and it deserves no further halving.

6.2. Relaxing the feasibility condition

The missed contraction of the starting search space $[\mathbf{P}]_0$ can also be due to a too tight feasibility condition. This algorithm inability in reaching a desired contraction level can be used as a switch from the basic B&B smart algorithm to a smarter one. In particular, the switch can also be driven by checking the frequency range where the model is unable to give an expected contraction of $[\mathbf{P}]_0$.

The presence of noise affecting experimental data can be managed by "relaxing" the feasibility condition (15). Instead of requiring that it holds *for all frequencies*, one may require it to hold *for almost all frequencies*, excluding a small number of points. More formally, introducing the set $\mathcal{N}_r \subset \{1, \ldots, N\}$, having $N_r < N$ elements, the *relaxed feasibility condition* can be stated as follows:

Relaxed feasibility condition.

$$[R_{\mathrm{exp},k}] \cap [R_{\mathrm{F}}(\mathbf{P}, \omega_k)] \neq \emptyset \quad \text{for } k \in \mathcal{N}_r \tag{17a}$$

$$[X_{\mathrm{exp},k}] \cap [X_{\mathrm{F}}(\mathbf{P}, \omega_k)] \neq \emptyset \tag{17b}$$

where $\mathcal{N}_r$ can arbitrarily be chosen in $\{1, \ldots, N\}$ at each step. From a practical point of view, a subset is feasible if the extended feasibility condition is fulfilled in a reduced number N_r of frequency points, allowing that the equations (15) are *not* fulfilled in a small number $M = N - N_r$ of points. In the following, $M \leq 5\%\, N$. The algorithm based on the extended and relaxed feasibility conditions will be named *Enhanced Smart B&B* (ESB&B) *algorithm*.

7. ESB&B identification working on noisy data

In this section, the ESB&B is applied to a real case of noisy FC experimental data obtained by EIS experiments. In real measurements, a high level of noise, located in the low-frequency range, e.g., tenths of Hertz, appears. If non-IA approaches are used, this noise has to be filtered out with a suitable signal processing. In this Section, it is shown that the proposed ESB&B inherently manages such a noise.

In order to have a straightforward 2D graphical representation of the ESB&B results, the interval codomain, that is the impedance computed by using Fouquet model, is plotted with the experimental EIS data, bounding them. The tighter the bound, the more accurate the results.

7.1. Case study 2: low noise level

A noisy experimental spectrum $\dot{Z}_{\text{exp}}$, obtained in the framework of the project [4] is shown in Figure 12. The measurement noise is more evident in the low frequency range. The spider plot shown in Figure 13 reveals that, up to the 9^{th} branching level, only $[R_\Omega]$ is contracted. From that level on, also the intervals $[R_{ct}]$, $[R_d]$ and $[\phi]$ are contracted. After the 19^{th} level, the ESB&B algorithm has contracted the initial search space by collecting the feasible subsets (in the relaxed sense), as shown in Table 4.

The following wrapping region is achieved:

$$\begin{aligned} [R_\Omega] &= 0.0411 \pm 9.50\% & [Q] &= 0.1383 \pm 27.68\% \\ [R_{ct}] &= 0.0704 \pm 11.10\% & [\phi] &= 0.8383 \pm 0.84\% \\ [R_D] &= 0.0643 \pm 10.25\% & [\tau_D] &= 0.1070 \pm 6.57\% \end{aligned} \tag{18}$$

The results is plotted in Figure 14. Once again, the interval identification is more tolerant to noise at low frequency, while in high frequency the contraction has bounded $\dot{Z}_{\text{exp}}$ much more tightly.

A further contribution to the identified interval widths comes from the inadequacy of the Fouquet model in bounding the experimental data on the whole frequency range. Indeed, the large Q span shown in (18) allows the blue circles to be bounded by the interval codomain of Fouqet model on the whole frequency range chosen for the analysis.

7.2. Case study 3: high noise level

The impedance spectrum shown in Figure 15 exhibits a significant noise level at low frequency, having an important impact on the identification

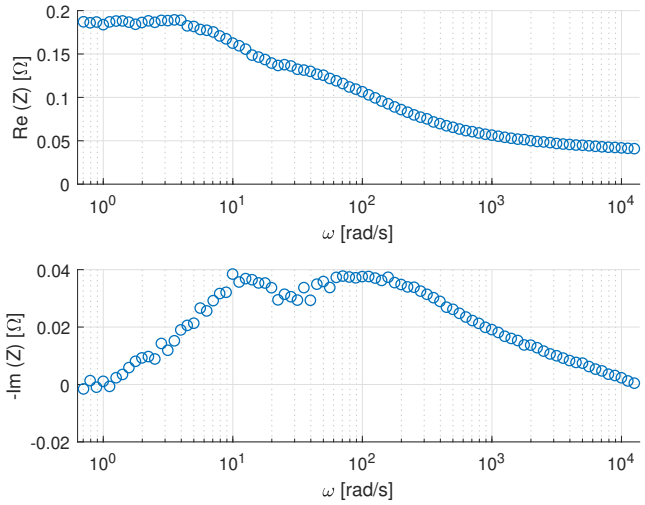

Figure 12: Case study 2: noisy impedance spectrum

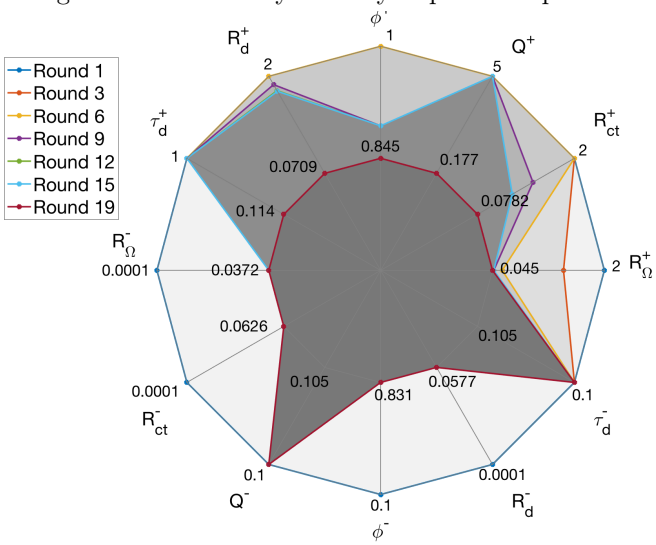

Figure 13: Case study 2: Spider plot showing the search space contraction.

results obtained through ESB&B algorithm. Indeed, the following wrapping

Branching level	Total subsets	Feasible subsets
1	1	1
3	40	20 (50 %)
6	40	20 (50 %)
9	13376	956 (7.2 %)
12	23176	8121 (35 %)
15	51192	49215 (96 %)
19	859712	195 (0.02 %)

Table 4: Case study 2: subsets classification up to the 19^{th} level.

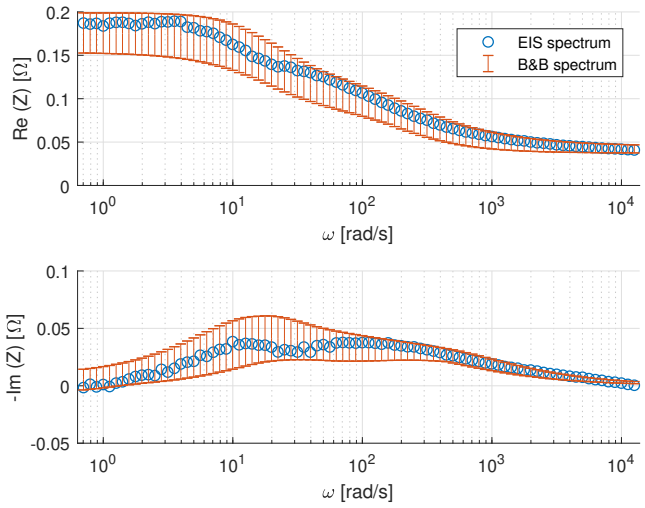

Figure 14: Case study 2: interval bounding of the experimental spectrum.

region W_{19} of the feasible subsets at 19^{th} branching level is achieved:

$$
\begin{aligned}
[R_\Omega] &= 0.0392 \pm 19.95\% & [Q] &= 0.1957 \pm 48.9\% \\
[R_{ct}] &= 0.1668 \pm 33.51\% & [\phi] &= 0.775 \pm 14.52\% \\
[R_D] &= 0.1153 \pm 66.04\% & [\tau_D] &= 0.3812 \pm 73.77\%.
\end{aligned} \tag{19}
$$

The results are plotted in Figure 16 and summarized in Table 5. By comparing Table 4 and Table 5, it is evident that, at the 19^{th} branching level, the number of feasible subsets in this latter case is one order of magnitude greater. As a consequence, the contraction characterising (19) cannot be as significant as the one in (18). The graphical counterpart of the large intervals in (19) are the large codomain (red ranges) in Figure 16.

Branching level	**Total subsets**	**Feasible subsets**
1	1	1
3	48	24
6	48	24
9	38080	1768
12	37584	17153
15	79136	23596
19	12439984	105865

Table 5: Case study 3: subsets classification.

As in the previous case, the identified subsets (19) are obtained by wrapping all the feasible intervals at the 19^{th} branching level in W_{19}. Such subsets could have been branched furthermore.

By taking from the wrapping region the following feasible subset:

$$\begin{aligned} R_\Omega &= 0.043065\,\Omega \pm 9.07\,\% & Q &= 0.1407 \pm 1.71\% \\ R_{ct} &= 0,1794\Omega \pm 0.06\,\% & \phi &= 0.80315 \pm 3.50\,\% \\ R_D &= 0.080175\Omega \pm 2.44\,\% & \tau_D &= 0.1281\,s \pm 21.9\,\%, \end{aligned} \tag{20}$$

the experimental data are bounded much more closely, as Figure 17 shows. The high sensitivity of the identified subset with respect to τ_D is confirmed.

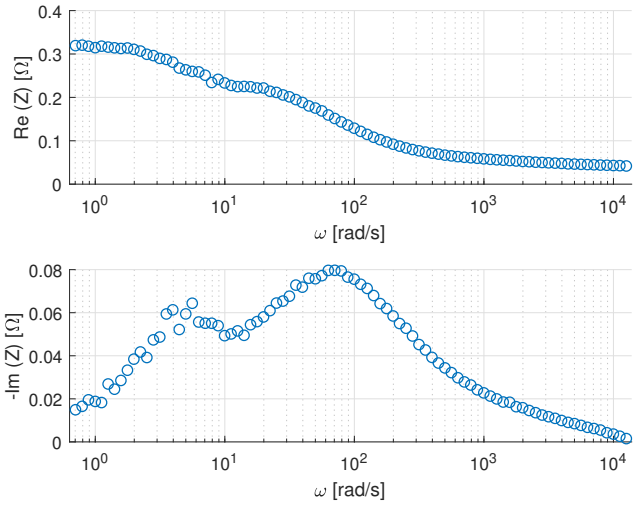

Figure 15: Case study 3: Experimental impedance spectrum.

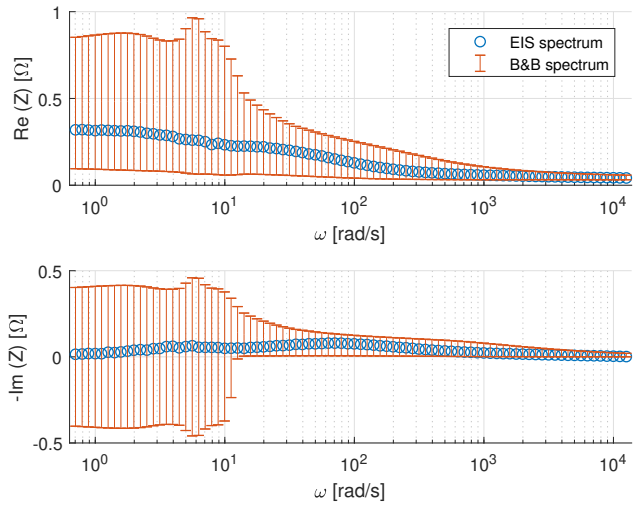

Figure 16: Case study 3: range bounding of the experimental spectrum in Figure 15

8. Discussion and remarks

The features of the proposed smart B&B algorithm are shown in Case study 1. The fictitious experimental data are generated by running the Fou-

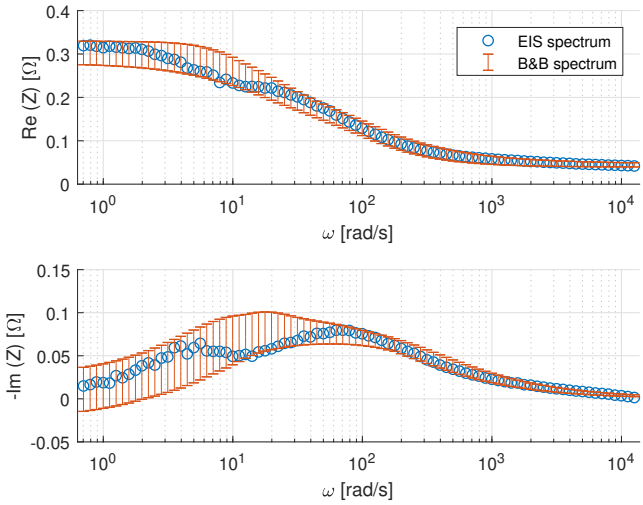

Figure 17: Case study 3: codomain of one selected feasible subset (20) of the wrapping region.

quet model, that is the same model used in the IA-based identification. This allowed to obtain the accurate results shown in Figure 10. The benefits deriving from the use of the proposed smart approach are evident, as the computational burden and the memory requirement are strongly reduced with respect to those required by the basic B&B approach.

In the examples of Section 7, experimental data affected by uncertainty are used. In this case, the adequateness of the equivalent circuit model adopted in the identification procedure is not known apriori and this might deeply affect the results. The innovative enhanced and relaxed feasibility conditions are effective, as shown in Figure 17, as the experimental data are tightly bounded.

On the basis of the achieved results, it is worth to remark the novel perspective application of the proposed method to FC monitoring and diag-

nostics.

First, the ESB&B approach can be applied in practical cases of interest, i.e., even in the presence of experimental spectra affected by measurement noise. In this case, the experimental data can be represented by a pair of IA-valued variables and the ESB&B approach, based on the relaxed feasibility condition (17), allows to bound these measurements, either in all the frequency points, or, for locally critical cases, in a subset of them.

Second, as it is shown in the Case study no. 2 and no. 3, the ESB&B method established a correlation between the parameter's range and the bounding level of the impedance spectrum. The bounding is typically broader at low frequency, in the region where the sinusoidal EIS experimental data typically exhibit higher noise. This noise is due to the difficulty of keeping the FC operating point constant during the minutes required by the EIS analysis at frequencies that very often are as low as few tenths of millihertz (this result is consistent with [25]). As a consequence, the proposed parametric identification process is naturally resilient to low frequency noise.

Third, it was pointed out above that, at each branching level, the wrapping region of all the feasible subsets (either extended or relaxed), that is an hyper-rectangle, may include unfeasible solutions. This can be ascribed to the properties of the union set of feasible subsets: it could be non-convex or non-connected. This information is very useful for monitoring and diagnostic purposes. For the sake of simplicity, refer to Case study 3. Suppose that the parametric identification is done when the FC works in normal conditions, with the results in (19), corresponding to the associated ranges in Figure 17. If its experimental FC impedance spectrum, that might vary with time, keeps

bounded inside the red bars in Figure 17 during the FC life and for the same operating point, the Fouquet model parameters do not exceed their limits (19). Such limits represent the safe operation of the FC and their variation can be related to specific degradation phenomena or to control actions for adjusting the FC operating conditions. This avoids to repeat the parametric identification of the refreshed EIS impedance spectrum, that is usually done by many diagnostic methods in literature as soon as a novel spectrum is acquired.

Fourth, the proposed method is also useful to evaluate the adequateness of the Fouquet model for the representation of the FC impedance spectrum, by revealing an unsatisfactory contraction of the initial search space.

Finally, it is worth to remark the broad applicability of the ESB&B method. It can effectively be applied to other EIS-based spectra, measured, for instance, on Solid-oxide FC [3, 27] or even on batteries and supercapacitors [28], where similar identification problems are in place on EIS spectra. Indeed, in the paper it is shown that the main source of results inaccuracy deriving from the use of IA is in the non linearity of some terms appearing in (4), which are related to the presence of the Warburg impendace and to the constant phase element. These latter terms also appear in battery impedance, e.g., see [29], and in super-capacitors frequency models, e.g., see [30]. Consequently, the authors are confident that the proposed approach has the potential to be exported also to these other systems even for state-of-charge monitoring purposes.

9. Conclusions

In this paper, an innovative interval analysis branch and bound method for parametric identification of a fuel cells model is proposed. The method is applied by modelling the fuel cell as a Fouquet impedance. The approach is deterministic and starts from a search space that is progressively contracted by using branching rules towards a parameters subset that gives an interval-valued impedance spectrum bounding of the experimental data. The approach is validated in an emulated framework and tested also with real experimental fuel cell spectra, measured with a sine-based electrochemical impedance spectroscopy. Three different version of the algorithm are discussed, progressively refined to face the presence of noise on experimental data. The method exhibits interesting features for its application to fuel cells monitoring and diagnostics, thus aimed at improving the stack performance and energy production over a longer lifetime. Further work is in progress to optimise the implementation of the method onto low-cost embedded systems and to develop diagnostic criteria, based on a large number of real fuel cell experimental data.

10. Acknowledgments

This work has been supported by FARB funds of the University of Salerno and European Project HEALTH-CODE (grant # 671486).

References

[1] A. L. Facci, S. Ubertini, Analysis of a fuel cell combined heat and power plant under realistic smart management scenarios, Applied Energy 216

(2018) 60 – 72. doi:https://doi.org/10.1016/j.apenergy.2018.02.054.
URL http://www.sciencedirect.com/science/article/pii/S0306261918301806

[2] M. Jouin, M. Bressel, S. Morando, R. Gouriveau, D. Hissel, M.-C. Péra, N. Zerhouni, S. Jemei, M. Hilairet, B. O. Bouamama, Estimating the end-of-life of pem fuel cells: Guidelines and metrics, Applied Energy 177 (2016) 87 – 97. doi:https://doi.org/10.1016/j.apenergy.2016.05.076.
URL http://www.sciencedirect.com/science/article/pii/S0306261916306729

[3] T. Zhang, P. Wang, H. Chen, P. Pei, A review of automotive proton exchange membrane fuel cell degradation under start-stop operating condition, Applied Energy 223 (2018) 249 – 262. doi:https://doi.org/10.1016/j.apenergy.2018.04.049.
URL http://www.sciencedirect.com/science/article/pii/S030626191830607X

[4] Real operation pem fuel cells health-state monitoring and diagnosis based on dc-dc converter embedded eis, Tech. rep., european H2020 project (2015).
URL https://pemfc.health-code.eu/

[5] J. R. Macdonald, W. B. Johnson, Fundamentals of impedance spectroscopy, Impedance Spectroscopy: Theory, Experiment, and Applications, Second Edition (2005) 1–26.

[6] S. M. R. Niya, M. Hoorfar, Study of proton exchange membrane fuel cells using electrochemical impedance spectroscopy technique–a review, Journal of Power Sources 240 (2013) 281–293.

[7] V. Subotić, B. Stoeckl, V. Lawlor, J. Strasser, H. Schroettner, C. Hochenauer, Towards a practical tool for online monitoring of solid oxide fuel cell operation: An experimental study and application of advanced data analysis approaches, Applied Energy 222 (2018) 748 – 761. doi:https://doi.org/10.1016/j.apenergy.2018.03.182.
URL http://www.sciencedirect.com/science/article/pii/S0306261918305324

[8] M. Kandidayeni, A. Macias, A. Amamou, L. Boulon, S. Kelouwani, H. Chaoui, Overview and benchmark analysis of fuel cell parameters estimation for energy management purposes, Journal of Power Sources 380 (2018) 92 – 104. doi:https://doi.org/10.1016/j.jpowsour.2018.01.075.
URL http://www.sciencedirect.com/science/article/pii/S0378775318300752

[9] R. Petrone, Electrochemical impedance spectroscopy for the on-board diagnosis of pemfc via on-line identification of equivalent circuit model parameters, Ph.D. thesis, Università degli studi di Salerno, Italy (2014).

[10] N. Fouquet, C. Doulet, C. Nouillant, G. Dauphin-Tanguy, B. Ould-Bouamama, Model based pem fuel cell state-of-health monitoring via ac impedance measurements, Journal of Power Sources 159 (2) (2006) 905–913.

[11] K. Ettihir, L. Boulon, M. Becherif, K. Agbossou, H. Ramadan, Online identification of semi-empirical model parameters for pemfcs, International Journal of Hydrogen Energy 39 (36) (2014) 21165 – 21176. doi:https://doi.org/10.1016/j.ijhydene.2014.10.045.
URL http://www.sciencedirect.com/science/article/pii/S0360319914028481

[12] W. Gong, X. Yan, X. Liu, Z. Cai, Parameter extraction of different fuel cell models with transferred adaptive differential evolution, Energy 86 (2015) 139 – 151. doi:https://doi.org/10.1016/j.energy.2015.03.117.
URL http://www.sciencedirect.com/science/article/pii/S0360544215004661

[13] B. Davies, L. Jackson, S. Dunnett, Expert diagnosis of polymer electrolyte fuel cells, International Journal of Hydrogen Energy 42 (16) (2017) 11724 – 11734. doi:https://doi.org/10.1016/j.ijhydene.2017.02.121.

[14] R. E. Moore, Interval Analysis, Prentice-Hall, Englewood Cliffs, N.J., 1966.

[15] T. Machado-Coelho, A. Machado, L. Jaulin, P. Ekel, W. Pedrycz, G. Soares, An interval space reducing method for constrained problems with particle swarm optimization, Applied Soft Computing 59 (2017) 405 – 417. doi:https://doi.org/10.1016/j.asoc.2017.05.022.
URL http://www.sciencedirect.com/science/article/pii/S1568494617302752

[16] C. Yang, Z. Lu, Z. Yang, K. Liang, Parameter identification for structural dynamics based on interval analysis algorithm, Acta Astronautica 145 (2018) 131 – 140. doi:https://doi.org/10.1016/j.actaastro.2018.01.038.
URL http://www.sciencedirect.com/science/article/pii/S009457651731408X

[17] P. Li, W. Xu, D. Yang, An inversion design method for the radome thickness based on interval arithmetic, IEEE Antennas and Wireless Propagation Letters 17 (4) (2018) 658–661. doi:10.1109/LAWP.2018.2810281.

[18] S. Kiel, E. Auer, A. Rauh, Uses of gpu powered interval optimization for parameter identification in the context of so fuel cells, Vol. 9, 2013, pp. 558–563. doi:10.3182/20130904-3-FR-2041.00169.

[19] E. Auer, L. Senkel, S. Kiel, A. Rauh, Control-oriented models for so fuel cells from the angle of v&v: Analysis, simplification possibilities, performance, Algorithms 10 (4) (2017). doi:10.3390/a10040140.
URL http://www.mdpi.com/1999-4893/10/4/140

[20] A. Rauh, T. Dötschel, E. Auer, H. Aschemann, Interval methods for control-oriented modeling of the thermal behavior of high-temperature fuel cell stacks, IFAC Proceedings Volumes 45 (16) (2012) 446 – 451, 16th IFAC Symposium on System Identification. doi:https://doi.org/10.3182/20120711-3-BE-2027.00374.
URL http://www.sciencedirect.com/science/article/pii/S147466701537991X

[21] A. Rauh, L. Senkel, H. Aschemann, Sensitivity-based state and parameter estimation for fuel cell systems, IFAC Proceedings Volumes 45 (13) (2012) 57 – 62, 7th IFAC Symposium on Robust Control Design. doi:https://doi.org/10.3182/20120620-3-DK-2025.00071.
URL http://www.sciencedirect.com/science/article/pii/S1474667015376631

[22] C. A. Floudas, Deterministic Global Optimization. Theory, Methods and Applications, Kluver Academic Publishers, London, UK, 1999.

[23] P. Moçotéguy, S. Pellegrino, B. Ludwig, A. Esposito, B. Iwanschitz, A. Mai, A novel approach to analyse incomplete design of experiments. application to the study of the influence of operational parameters on

the performance of a solid oxide fuel cell based micro-combined heat and power system, International Journal of Hydrogen Energy (2018). doi:https://doi.org/10.1016/j.ijhydene.2018.11.029.
URL http://www.sciencedirect.com/science/article/pii/S0360319918335778

[24] S. K. Roy, M. E. Orazem, Error Analysis of the Impedance Response of PEM Fuel Cells, Journal of The Electrochemical Society (2007). doi:10.1149/1.2747533.

[25] A. Debenjak, P. Boškoski, B. Musizza, J. Petrovčič, D. Juričić, Fast measurement of proton exchange membrane fuel cell impedance based on pseudo-random binary sequence perturbation signals and continuous wavelet transform, Journal of Power Sources 254 (2014) 112 – 118. doi:https://doi.org/10.1016/j.jpowsour.2013.12.094.
URL http://www.sciencedirect.com/science/article/pii/S0378775313020831

[26] L. Jaulin, M. Kieffer, O. Didrit, E. Walter, Applied Interval Analysis, Springer Science & Business Media, 2001.

[27] Y. Zhang, Y. Chen, M. Yan, F. Chen, Reconstruction of relaxation time distribution from linear electrochemical impedance spectroscopy, Journal of Power Sources 283 (2015) 464 – 477. doi:https://doi.org/10.1016/j.jpowsour.2015.02.107.
URL http://www.sciencedirect.com/science/article/pii/S0378775315003523

[28] C. Zou, L. Zhang, X. Hu, Z. Wang, T. Wik, M. Pecht, A review of fractional-order techniques applied to lithium-ion batteries, lead-acid batteries, and supercapacitors, Journal of Power Sources 390 (2018)

286 – 296. doi:https://doi.org/10.1016/j.jpowsour.2018.04.033.
URL http://www.sciencedirect.com/science/article/pii/S0378775318303768

[29] X. Zhu, L. F. Macía, J. Jaguemont, J. de Hoog, A. Nikolian, N. Omar, A. Hubin, Electrochemical impedance study of commercial lini0.80co0.15al0.05o2 electrodes as a function of state of charge and aging, Electrochimica Acta 287 (2018) 10 – 20. doi:https://doi.org/10.1016/j.electacta.2018.08.054.

[30] S. Buller, E. Karden, D. Kok, R. W. D. Doncker, Modeling the dynamic behavior of supercapacitors using impedance spectroscopy, IEEE Transactions on Industry Applications 38 (6) (2002) 1622–1626. doi:10.1109/TIA.2002.804762.